> Manuscript ID TNANO-00252-2025.R1

Large-Area Field Enhancement via Plasmonic Hot-Grid in Nanocube Arrays

Anna Lee, *Senior Member, IEEE*, Sebastian Carrillo, Young Seok Shon, Aftab Ahmed, *Member, IEEE*

***Abstract*— Plasmonic nanoparticles have attracted considerable attention due to their ability to amplify local electric fields and generate hot-spots. These hot-spots are highly desirable for enhancing scattering and non-linear processes. Rough surfaces and sharp edges have been previously used for such applications. However, small hot-spot volume and inherent randomness limit their reliability and effectiveness. Here, we propose a design that utilizes interference of surface plasmon polaritons using array of nanocubes. We numerically study the analytical solutions of the metal-insulator-metal (MIM) geometry and conduct finite difference time domain simulations to investigate the optical response of the proposed design. The design offers over 1000-fold local field intensity enhancement which corresponds to over 10^6-fold Raman enhancement. We demonstrate field enhancement over a large area that we term the "hot-grid". The design uses the propagating odd surface plasmon polariton mode of MIM geometry produced by an array of nanocubes. The extremely small gap of 1 nm produces significant field enhancement, which is further amplified by constructive interference achieved by multiple reflections, similar to a Fabry-Perot cavity. These results highlight the promise of nanocube arrays for applications that demand significant electric field enhancement, including nonlinear optics, photonics, spectroscopy, sensing, and imaging.**

***Index Terms*— Hot-spot, MIM, Nanocube Array, Near field Enhancement, Plasmonics, SERS, SPP**.

This work was supported by the office of research and economic development through the 2024 summer student assistantship program at California State University of Long Beach. *(Corresponding authors: Anna Lee and Aftab Ahmed).*

Anna Lee, and Aftab Ahmed are with the Electrical Engineering department of California State University Long Beach, 1250 Bellflower Blvd, Long Beach, CA 90840 USA (e-mail: anna.lee@csulb.edu; aftab@csulb.edu).

Sebastian Carrillo is with the Mechanical and Aerospace Engineering department of California State University Long Beach (e-mail: sebastian.carrillo01@student.csulb.edu).

Young Seok Shon is with the Chemistry and Biochemistry department of California State University Long Beach (e-mail: Ys.shon@csulb.edu).

I. INTRODUCTION

THE unique capabilities of plasmonics have significantly advanced various fields including sensing, photovoltaics, sub-wavelength imaging, photocatalysis, optoelectronics, and biomedicine [1], [2], [3], [4]. The electric field of incident light exerts a force on the free electrons in metal nanoparticles and depending upon the size and shape of the particle, certain wavelengths of incident light can resonantly excite collective electron oscillations known as surface plasmons [5]. These collective oscillations result in the accumulation of large amounts of charge near the surface, enhancing the local electromagnetic field. These localized surface plasmon resonances (LSPR) are capable of providing strong enhancement of the electromagnetic field that can be used to amplify other optical phenomena that depend upon the electric field magnitude [2], [6], [7], [8]. Hot-spots are used to enhance various scattering processes that are inherently weak to observe, such as Raman scattering [9], [10], [11], [12] and also improve the efficiency of optical non-linear processes such as frequency conversion [13], [14]. The resonance modes of plasmonic nanoparticles are dependent on particle size, geometry, materials, and physical assortment [15], [16], [17], [18]. Recent advances in nanofabrication have provided unprecedented control over particle size, geometry, and composition, enabling the realization of new designs to enhance light-matter interactions via nanoscale engineering [19], [20], [21] . By designing the geometry, material, size, and spatial arrangement of nanoparticles, LSPR can be utilized to greatly control the absorption and reflection of light for desired applications [15], [22], [23]. Among these, nanocubes have received great attention due to their relatively sharp edges/corners, symmetry, and structural stability [24], [25], [26]. At resonance, the near-field intensities of these nanoparticles are significantly larger than the incident intensity. Additional field enhancement is achieved using a pair of particles (dimer), typically spheres, separated by a small gap [27], [28], [29]. Although dimers offer a significantly large field enhancement, they are typically formed in colloidal solutions, and the hot-spot volume is extremely small.

When plasmonic nanoparticles are arranged close to one another, coupling in the gaps between the nanoparticles can enhance the electromagnetic field intensity [16], [30], [31]. This method has been used in surface enhanced Raman scattering (SERS) applications to amplify weak Raman signals [32], [33], [34], [35] for sensing applications. Various methods and

substrates have been reported for the enhancement of local electric fields for SERS applications, but they utilize random structures with low reproducibility. This lack of reproducibility can be attributed to difficulties with limited uniformity, nanometer scale precision, and inability to use a top-down manufacturing approach [36], [37], [38].

A small gap between nanoparticles results in large field enhancement. Extremely high enhancement can be achieved by engineering vanishingly thin insulator layer. Top-down fabrication techniques are unable to produce such structures with very small gaps (< 2 nm). The other way around is the bottom-up approach of self-assembly; however, it is a common misconception that self-assembly of long-range arrays is a challenging and unreliable process. Here, we would like to emphasize that recent advances in nanofabrication techniques offer simple and reliable methods for the production of such arrays [39], [40], [41], [42]. In this work, we propose a design using nanocube array that offers a 1000-fold local field intensity enhancement. We numerically investigate such an array and demonstrate its potential for applications in areas requiring high electric field enhancement over large surface areas including SERS as a low-cost alternative for biomedical sensing, single molecule detection, and nonlinear optical processes.

II. Gap Plasmons and Interference

Design of reliable nanostructures that provide sufficient field enhancement while maintaining a large hot-spot volume is highly desirable. Surface plasmon polaritons (SPP) are surface waves that exist on metal-insulator interface and result in large local fields. These are propagating modes, and as such, enable the generation of large fields over a surface area, as opposed to small volumes produced by nanoparticles. The fields can be further enhanced by coupling two SPP waves. This can be achieved by a metal-insulator-metal (MIM) structure (Fig. 1). This configuration allows for the excitation of two SPP waves separated by the thickness of the insulator layer. The two SPP waves can couple if the insulator layer is sufficiently thin, producing even and odd SPP modes [43], [44]. The strength of the local electric field is inversely proportional to the thickness of the insulator layer and significantly large fields are produced by using vanishingly thin insulator layers. To quantify the field enhancement, the electric field of the SPP wave within the metal region in Fig. 1 for $x > d/2$, is given as (propagation along z-axis) [44]:

$$E_x = \frac{-\beta E_0}{\omega \varepsilon_2} e^{-k_2 x} e^{-i\beta z} \tag{1}$$

$$E_z = \frac{i k_2 E_0}{\omega \varepsilon_2} e^{-k_2 x} e^{-i\beta z} \tag{2}$$

where $k_i = \sqrt{\beta^2 - \varepsilon_i k_0^2}$ is the transverse wavenumber, ε_i is the permittivity the subscript i = 1, 2 specifies the insulator and metal regions respectively, and $k_0 = 2\pi/\lambda$ is the free space wavenumber. Stronger local fields can thus be produced via designing structures that support large values of β. The y-component of the electric field of the SPP wave is zero as the structure is in-variant in the y direction. Furthermore, only the y-component of the magnetic field is non-zero. These fields are evanescent in the direction normal to the interface, the modes are thus confined to the interface. The SPP propagation constant β can be obtained by applying boundary conditions, that is, continuity of tangential fields which leads to the following dispersion relations [44]:

$$\tanh\left(\frac{k_1 d}{2}\right) = -\frac{k_2 \varepsilon_1}{k_1 \varepsilon_2} \tag{3}$$

$$\tanh\left(\frac{k_1 d}{2}\right) = -\frac{k_1 \varepsilon_2}{k_2 \varepsilon_1} \tag{4}$$

Here d represents the thickness of the insulator layer and ε_2 is the dielectric function of metal. Equations 3 and 4 are the odd and even SPP modes, respectively. It is important to recognize that the odd mode exists for vanishingly small values of d. Decreasing the thickness of the insulator layer brings the two metal surfaces closer together which results in stronger coupling of the SPP waves on the two interfaces. The consequence of this stronger coupling is tighter confinement via larger k_i resulting in a larger value of β. Advantages of this large propagation constant include smaller wavelength (focusing of light) and larger local fields as suggested by Equation 1. Fig. 1 shows the odd solutions for varying insulator thicknesses of the MIM structures, formed using gold and silver. These results are for an infinite structure along y-axis as well as z-axis and as such $\partial/\partial y = 0$ and there are no reflections due to guide termination. It is noted that the even mode does not exist for very thin insulator layers, and as such, only the odd mode is of interest here. The propagation constant $\beta = k_0 n_{eff}$ is a complex quantity, the real part of which signifies the propagating mode, and the imaginary part represents loss or decay of the SPP wave along the direction of propagation. Field enhancement benefits from thinner insulator layers via larger values of Real(*neff*), however, losses in the metal regions

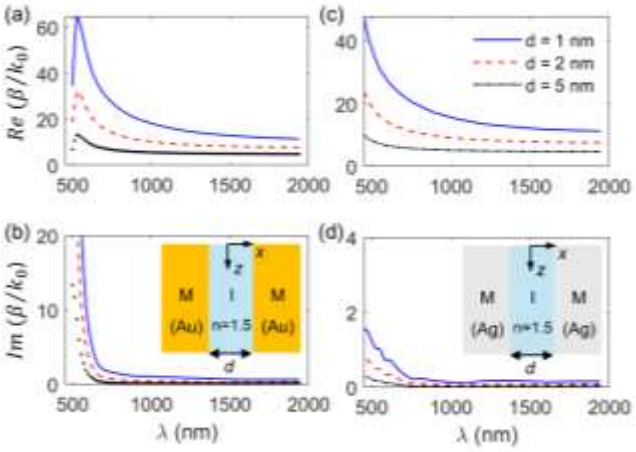

Fig. 1. Real and imaginary parts of the effective index of the odd SPP mode in a MIM nanostructure for three different insulator layer thicknesses, 1 nm (solid blue), 2 nm (dashed red) and 5 nm (dash-dot black). (a) and (b) present the dispersion curve of gold whereas (c) and (d) of silver. The structure is infinite in z direction.

become more significant at shorter wavelengths, severely limiting the propagation lengths of the SPP waves.

Here we present a scheme to significantly enhance the local fields of the planar MIM structure without compromising the volume of hot-spot region. We suggest the constructive interference of a number of these MIM SPP waves. For this purpose, we propose the formation of a cavity causing multiple reflections and formation of a standing wave within the cavity. Constructive interference is achieved when the round-trip phase acquired becomes an integer multiple of 2π. The phase acquired by the SPP wave over a distance l is $Real(\beta)l$, as such the length of the cavity can be adjusted to produce resonance at desired wavelength. Larger β values can amplify the local fields, however, the associated increase in $Imag(\beta)$ results in decaying amplitudes and thus prohibits the build-up of standing-wave fields within the cavity. Results of Fig. 1 suggest use of a thin insulator layer and operating in the spectral region $\lambda > 650\,nm$ (for gold) and $\lambda > 500\,nm$ (for silver). This allows for better field enhancement while maintaining sufficiently small losses to enable SPP wave interference.

Fabrication of a thin insulator layer (d approaching 1 nm) is challenging for top-down fabrication processes. Typically, top-down fabricated designs offer reproducible and reliable results, however, milling and etching processes are not able to produce features that require very high spatial resolution. Self-assembly of nanoparticles, on the other hand, can achieve the required gap size between metal nanoparticles. Here, we investigate an array of nanocubes with a gap of 1 nm between neighboring particles. The gap plays the role of the insulator layer sandwiched between two metal cubes. The length l of the cavity is determined by the edge length of the cube which thus dictates the resonance wavelengths. Fig. 2 shows the proposed structure of an array of nanocubes with edge length l. The design is sensitive to the gap dimension and a precise control of d is required for desired wavelength operation. Recent advances in the self-assembly process allow for the creation of Long-range, mono-layer arrays

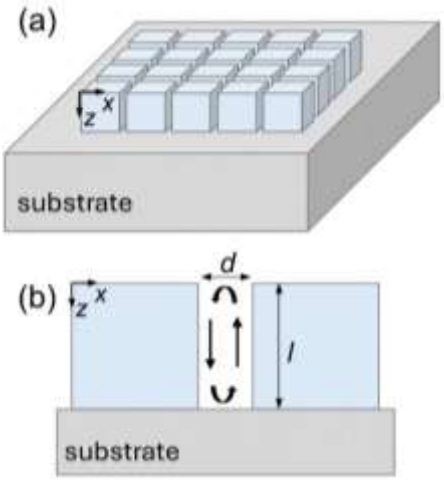

Fig. 2. (a) An array of metal nanocubes of edge length l and gap d between the cubes, with $l \gg d$. The incident light propagates along the positive z-axis and excites a SPP wave in the gap region. An effective refractive-index mismatch at $z = 0$ and $z = l$ causes reflection of the SPP wave forming a 1D cavity.

with very small (≈ 1 nm) and precisely controlled values of d [41], [45], [46].

It should be noted that the results in Fig. 1 represent an MIM structure that does not vary in the y-direction, however these results may be used to describe the response of the structure in Fig. 2 provided that the cube is significantly larger than the gap size $l \gg d$. In Fig. 3, we compare the SPP mode profiles of the MIM structure (Eq. 1 and 2) with that of the nanocube array obtained using FDTD simulations. Equations 1 and 2, show the fields in the metal region ($x > d/2$), similar exponentially decaying fields are expected in the ($x < -d/2$) regions due to symmetry. The fields within the insulator region consist of hyperbolic functions and are obtained via matching tangential fields across the two interfaces. Fig. 3a, shows the two non-zero electric field components of the odd SPP mode in the MIM structure at two different wavelengths (λ = 550 nm and 650 nm). The metal region is silver (shaded region in Fig. 3a) whereas the insulator region has an index of 1.5. The component along the direction of propagation (*Ez*) is an odd function of x confirming the odd vector parity of the SPP mode. More rapid decay of electric field is expected (Eq. 1 and 2) at shorter wavelengths due to larger values of SPP wavevector. The normal component (*Ex*) is discontinuous across the boundary and changes sign due to negative permittivity of metal region. Fig. 3b, shows the FDTD results of a silver nanocube (75 nm edge length) array midway inside the cavity, *z = l/2*, at 650 nm wavelength. The gap size is 1 nm with refractive index 1.5. The observed field profiles within the nanogaps match well with the analytical MIM-SPP mode, confirming the excitation of the odd SPP mode in the nanocube array.

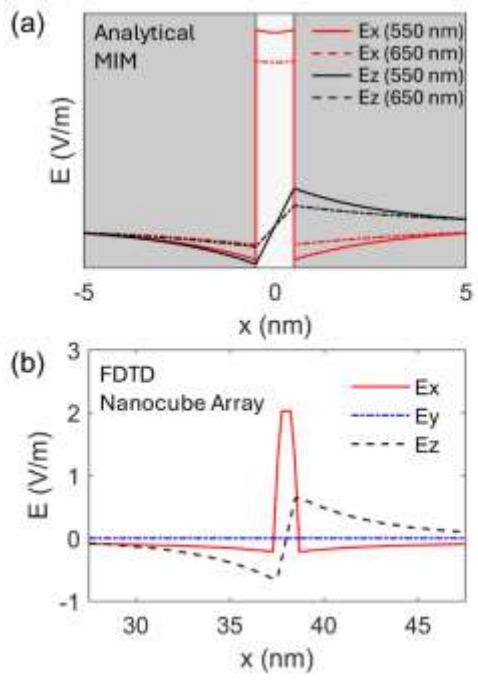

Fig. 3. (a) Analytical solution showing electric field of the odd SPP mode in MIM structure at λ = 550nm and 650nm. The metal region is silver, and the insulator gap is 1nm wide with index of 1.5. (b) Electric field within the cavity made by an array of silver nanocubes with *l* = 75nm, *d* = 1nm and gap index = 1.5 at λ = 650nm.

It is noted here that SPPs cannot be directly excited on a flat metal-dielectric interface by incident light due to the momentum mismatch. Typical methods for excitation include prism coupling, diffraction gratings, random surface roughness or fabricated localized scatterers [44]. These methods enable the excitation of in-plane SPP waves on the metal/dielectric interfaces, that is, SPP wavevector is in the xy-plane in Figure 2. In our case, the periodic nanocube array serves as the coupling mechanism, enabling the excitation of SPP modes. The MIM-SPP mode is along z-axis and is larger in magnitude than the in-plane SPP wavevector resulting in red-shifted resonance. Past studies demonstrate that structured metallic surfaces, including nanohole and nanoslit arrays, can support and couple to a range of SPP modes under normal incidence. In this regard, the original work by Ebbesen *et al.* on extraordinary optical transmission through subwavelength nanohole arrays suggested the involvement of SPPs [47]. However, the transmission peaks were red shifted from their expected spectral location. Further, a dip in transmission was observed at wavelengths that corresponded to the excitation of in-plane SPP mode. To explain the observed red-shift and also shed light on coupling of light to the SPP modes, K. G. Lee *et al.* studied thin nanoslits in metal films [48]. These results confirm the excitation of various SPP modes in nanohole arrays and slits in metallic structure. In addition, the nanocube square array studied here offers a grating like pattern, however the groves depth (l) is significantly larger than a typical grating and is almost equal to the period of the array. Such a design can also allow for the excitation of SPP waves within the groves as reported by Hooper and Sambles [49].

An additional advantage of the design in Fig. 2 is the self-formation of the reflecting boundaries at $z = 0$ and $z = l$. The effective refractive-index mismatch at these boundaries results in partial reflection of the incident SPP mode which enables the interference of SPP waves. For effective utilization of this interference phenomenon, it is necessary to maintain low losses and high reflection coefficient. A 1D cavity is naturally formed and the length of the cavity is equal to the edge length of the nanocube.

III. Methodology, Results and Discussion

The array of nanocubes is modeled by numerically solving full 3D wave equation using a commercial software based on finite difference time domain (FDTD) method from Ansys-Lumerical. The FDTD solution is rigorous and does not employ any assumptions or simplifications such as the invariance of structure in y-direction that was used to produce the results of Fig. 1. FDTD simulations accurately capture the effects of periodicity in both transverse directions. Taking advantage of the periodicity of the electromagnetic fields within the array, a unit cell is modeled along with periodic boundary conditions to calculate the response of the entire array.

Here, we first compare the optical response of a single nanocube and that of an array of nanocubes. To calculate the absorption and scattering cross-sections of single nanoparticles, the formalism of total field scattered field is employed in FDTD. Absorption of array is calculated using the reflection and transmission spectra of the array. Different sizes of nanocubes are investigated to explore the effects of cavity length (l) and gap size (d). To avoid erroneous results due to sharp edges, a 3 nm radius of curvature is used to round the edges and corners. The 1 nm gap is filled with Polyvinylpyrrolidone (PVP) with a refractive index of n = 1.5. The MIM nanostructure is placed on a glass substrate with an index of refraction of n = 1.54 and a plane wave source is normally incident onto the array. The material properties of Ag were modeled using the experimental values reported by Johnson and Christy [50].

The response of a single particle is primarily determined by the localized surface plasmon resonance (LSPR) which is weakly dependent on particle size. In the small particle size regime, the quasistatic approximation shows that this resonance is independent of particle's size, however, the resonance slightly shifts red as the particle size increases and the quasistatic approximation breaks down. For a spherical nanoparticle, Mie theory can be used to calculate the LSPR, Equation 5 and 6 below, give the absorption and scattering cross-section in the context of LSPR [51]. These cross-sections are a measure of the efficiency with which nanoparticles absorb and scatter light.

$$C_{abs} = 4\pi k a^3 Im\left[\frac{\varepsilon - \varepsilon_m}{\varepsilon + 2\varepsilon_m}\right] \tag{5}$$

$$C_{scatt} = \frac{8\pi}{3} k^4 a^6 \left[\frac{\varepsilon - \varepsilon_m}{\varepsilon + 2\varepsilon_m}\right]^2 \tag{6}$$

Here ε and ε_m are the permittivities of the nanoparticle and the surrounding medium respectively. Both scattering and absorption are resonantly enhanced, and the resonance condition is $\varepsilon = -2\varepsilon_m$ which is seen to be independent of particle size. Non-spherical nanoparticles typically require the use of numerical methods to calculate plasmon resonances and cross-sections. Here, we used FDTD method to calculate these cross-sections of a single silver nanocube with rounded edges and corners. Fig. 4 shows the absorption, scattering and extinction cross-sections of a 75 nm and a 100 nm Ag nanocube with LSPRs at 480 nm and 530 nm respectively. The higher order resonances occur at even shorter wavelengths and are not of interest here [52]. It is noted that optical response of isolated nanocubes primarily occurs at wavelengths shorter than 600 nm and no significant optical activity is observed at longer wavelengths. On the other hand, an array of such cubes can produce resonant optical activity at much longer wavelengths.

The SPP of the MIM structure is highly sensitive to particle size and gap between adjacent particles. Smaller gaps results in large β which causes larger phase acquisition over short distances. This causes the resonance to red shift and a significantly longer wavelength can be made to resonate within the MIM cavity. For instance, according to microwave theory, a cavity formed by 50 nm cubes shall resonate at a wavelength of 100 nm, ignoring reflection phase. However, plasmonic

effects causing large β and short guide wavelength, can shift the resonance of the same structure to significantly longer

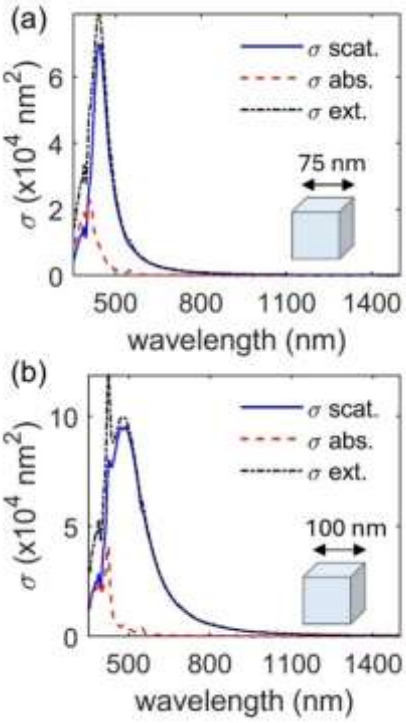

Fig. 4. Scattering, absorption and extinction spectra of (a) 75 nm and (b) 100 nm single silver nanocube.

wavelengths as seen in the results of Fig. 5. Different cube lengths, 50 nm, 72 nm, 75 nm and 78 nm are investigated to demonstrate the tunability of the structure and sensitivity of resonance wavelength to cavity length. Electric field intensity enhancement and absorbance of the arrays are shown in Fig. 5b and 5c respectively. Fig. 5a shows the electric field profiles of the fundamental (λ = 1690 nm) and first higher order (λ = 1071 nm) modes of a 75 nm nanocube array in the gap region. Incident light is x-polarized and the scalebar is logarithmic, demonstrating over 1000 times field enhancement produced by both modes. The gap region is 1 nm wide and has a refractive index of 1.5. The substrate surface is at $z = 0$. The x-polarized incident light excites the gap plasmon mode with $Ey = Hx = Hz = 0$. The normalized intensities as a function of z for the two dominant modes for two different gap sizes, 1 nm solid blue and 2 nm dashed red, are also shown in Fig 5a. The fundamental mode exhibits one whereas the higher order mode shows two nodes.

To investigate the resonance sensitivity to nanoparticle size, Fig. 5 shows a wavelength shift of 108 nm in response to particle's edge length change from 72 nm to 78 nm. This represents a size variation of about 8%. Recent advances in nanofabrication methods offer particle size control better than 8%. Experimental results will show a slight peak broadening due to size dispersion. Applications such as Raman scattering process benefit from this peak broadening as both excitation and scattering events are amplified.

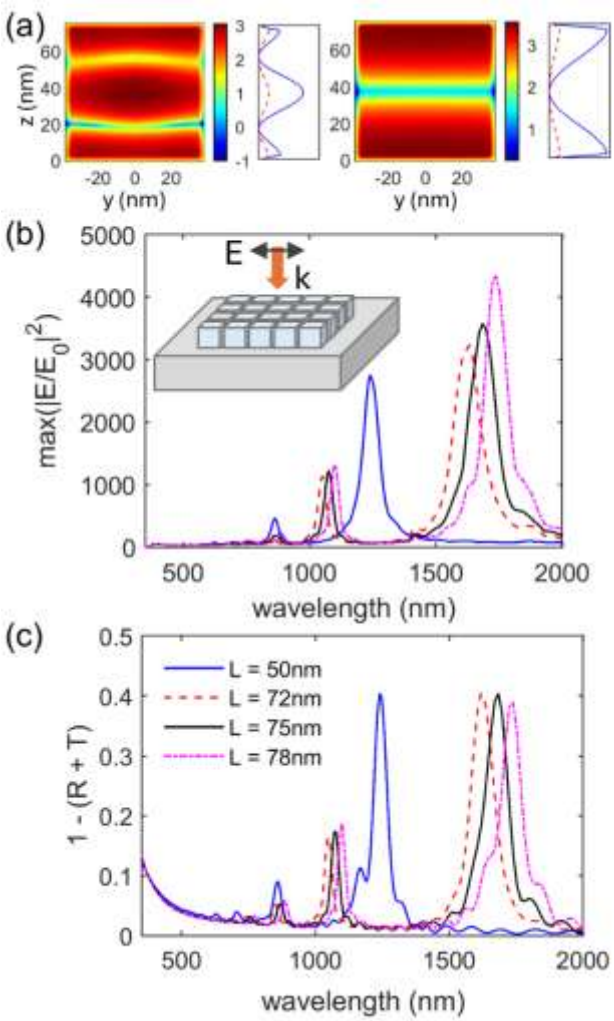

Fig. 5. (a) Electric field profiles of the fundamental (λ = 1690 nm) and first higher order (λ = 1071 nm) modes of a 75 nm silver nanocube array (log-scale). The gap region is 1 nm wide and has a refractive index of 1.5. Intensity profiles of the two dominant modes vs z for 1 nm gap (solid blue) and 2 nm gap (dashed red). Local electric field intensity enhancement (b) and absorbance (1 – (R + T) spectra (c) of silver nanocube arrays. Cube edge lengths *L* are 50 nm (solid blue) 72 nm (dashed red), 75 nm (solid black) and 78 nm (dash-dotted magenta).

The resonances of larger nanoparticle array occur at longer wavelengths primarily due to cube's dimension. The fundamental resonance represents a standing wave created by the interference of two counter propagating waves with a round-trip phase of 2π. Higher order resonances are formed by round trip phase acquisition of $4\pi, 6\pi$ ... . The formation of standing waves within these large number of nanocavities not only enhance local fields but also provide a large area over which high electric field is produced.

A correlation between field enhancement and absorbance is evident from the results of Fig. 5. Power absorbed per unit volume in a material can be calculated as, $P_{abs} = \pi c|E|^2 Imag(\varepsilon)/\lambda$. Absorption is thus proportional to the electric field intensity and inversely proportional to wavelength. Considering the 72 nm and 78 nm arrays, results in Fig. 5 show an increase in field intensity (from 3,220 to 4,330) as well as resonance shift (from 1,630 nm to 1,738 nm). Intuitively, one would expect an increase in absorption due to

stronger field intensity, however, the overall effect is a slight reduction in absorption as particle size increases. The shift in resonance alone is not sufficiently large to account for the reduced absorption and the imaginary part of permittivity of silver also does not explain the effect. To further investigate this effect, we present the transmission and reflection spectra in Fig. 6. It is observed that larger particle array allows for higher transmission and reduced reflection, which again is contrary to expectation. A MIM waveguide which is inherently lossy, shall absorb more energy as the length of the waveguide is increased. However, our results show the opposite, demonstrating the complex interactions of light and nanoarray. The slight reduction in absorption might be due to reduced penetration depth of electric field in the conducting region at longer wavelengths. Another interesting feature of the nanoarray is the behavior of the higher order modes shown in Fig. 5 and Fig. 6. These modes exhibit high electric field intensity as well as absorption. However, almost zero transmission is observed, the incident energy is either reflected (≈80%) or absorbed (≈20%) by the array. These are the dark modes of the structure that produces large field enhancement but do not couple to free space radiation.

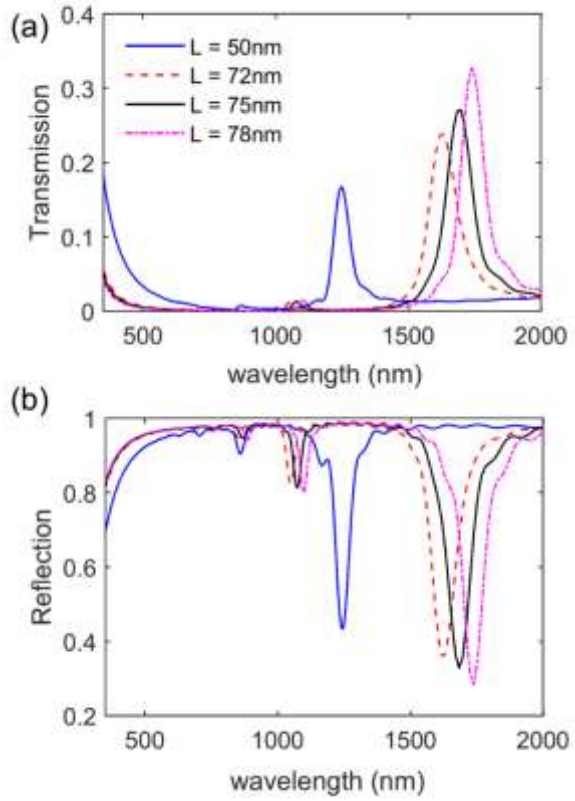

Fig. 6. Transmission (a) and reflection (b) spectra of silver nanocube arrays. Cube edge lengths L are 50 nm (solid blue) 72 nm (dashed red), 75 nm (solid black) and 78 nm (dash-dotted magenta). The gap region is 1 nm wide and has a refractive index of 1.5.

The proposed structure is independent of incident polarization due to its symmetry in the transverse plane. For instance, an x-polarized incident wave will generate SPP modes with Ex and Ez components in gap regions parallel to y-axis, whereas a y-polarized incident wave will result in Ey and Ez components in gaps parallel to x-axis. As such an unpolarized light will excite SPP modes in all gap regions and create a grid of hot-spots ("hot-grid").

The higher order modes exhibit a greater number of nodes and occur at shorter wavelengths as expected. The resonance produces field profiles with anti-nodes at the surface of the nanoarray which is beneficial for many applications, particularly sensing applications requiring the molecule of interest to be in close proximity of the hot-spot. The local electric field intensity $E^2 = (E_x^2 + E_y^2 + E_z^2)$ within the gap regions show enhancement of more than 1000 times compared to that of the incident light which can improve the efficiencies of optical processes by three orders of magnitude. Further, the design is ideal for SERS as Raman enhancement factor is proportional to the fourth power of the local electric field. Thus the Raman enhancement offered by this design exceeds 10^6.

Gap size d is another parameter that determines the performance of the nanoarray. Experimentally, this gap size can be precisely controlled via capping ligands. A smaller gap size results in tighter confinement of the SPP mode resulting in shorter guide wavelengths, larger local fields and larger wavenumber β. Plasmon resonance is highly sensitive to gap size and a decrease in gap size significantly shifts the plasmon resonance to longer wavelengths.

Fig. 7 shows the electric field intensity enhancement of a 50 nm silver nanocube array with different gap sizes d. We observe about 350 nm shift in resonance as the gap size reduces from 1.5 nm to 1 nm. At the same time, the electric field intensity increases from 1000 to 2800 as the gap size decreases.

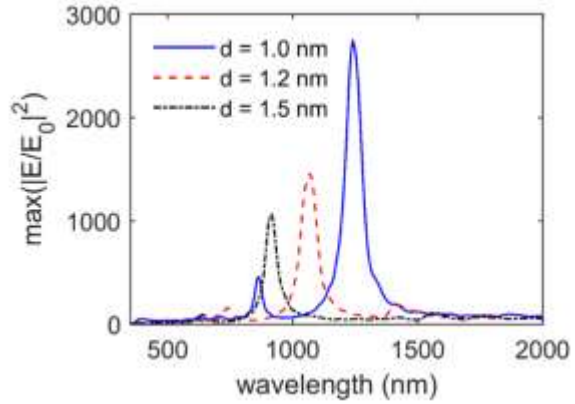

Fig. 7. Electric field intensity enhancement of a 50 nm silver nanocube arrays with gap 1nm (solid blue), 1.2 nm (dashed red) and 1.5 nm (dashed dot black). The fundamental plasmon resonance shifts by approximately 350 nm in response to a gap size change from 1.5 nm to 1 nm.

The results presented above are based on silver nanocube arrays. Similar results are expected from gold arrays. Silver offers desirable optical properties with its interband transitions in the ultraviolet region; however, silver suffers from oxidation. Gold can thus be used as an alternative plasmonic material for applications where oxidation prohibits the use of silver. Compared to silver, gold's optical response is desirable at wavelengths longer than 500 nm. The high losses in gold at shorter wavelengths cause the SPP waves to decay rapidly and

thus prohibit energy buildup in the cavity. Fig. 8 shows the absorption and electric field intensity profile of a 75 nm gold nanocube array. The fundamental resonance of the cavity is observed at 1727 nm indicated by a peak in absorption as well as by the amplification (1000 times) of local electric field intensity. The absorption peak near 500 nm arises due to the interband transitions resulting in a rapid decay of energy and therefore the resonant enhancement of electric field is not observed. The inset in Fig. 8b shows the intensity profile of the fundamental mode at the resonant wavelength of 1727 nm.

In addition to SERS, other optical processes such as nonlinear optical processes can benefit from field enhancement over a large surface area. In some cases, it is not feasible to take advantage of the high local field within the gap region and as such field profile over the top surface of the array is of primary interest. The electric field intensity 0.2 nm above the surface of the 75 nm silver nanoarray normalized to the incident intensity $\left|E/E_0\right|^2$ is shown in Fig. 9. Here, the incident light is unpolarized which is approximated by performing two simulations with orthogonal linear polarizations. Due to linearity of Maxwell's equations the net response is obtained by averaging the two responses, that is $|E_{net}|^2 = 0.5\left|E_{0\,deg}\right|^2 + 0.5\left|E_{90\,deg}\right|^2$. It is noted here that this method of incoherent superposition of two orthogonal polarizations is an approximation and does not rigorously represent unpolarized light. The unpolarized response forms a square grid of hot-spots which at a distance of 0.2 nm above the array, produces intensity enhancement larger than 100 times as shown in Fig. 9. It is noted that the individual hot-spots are larger than the 1 nm gap size and these hot-spots spread as we move away from the array's surface. This also suggests that the field enhancement would be larger than 100 near the surface of the array and the hot-spot volume would decrease. Also, if the incident light is linearly polarized along one of the axes of the array, then instead of the square grid, a liner gird will be produced.

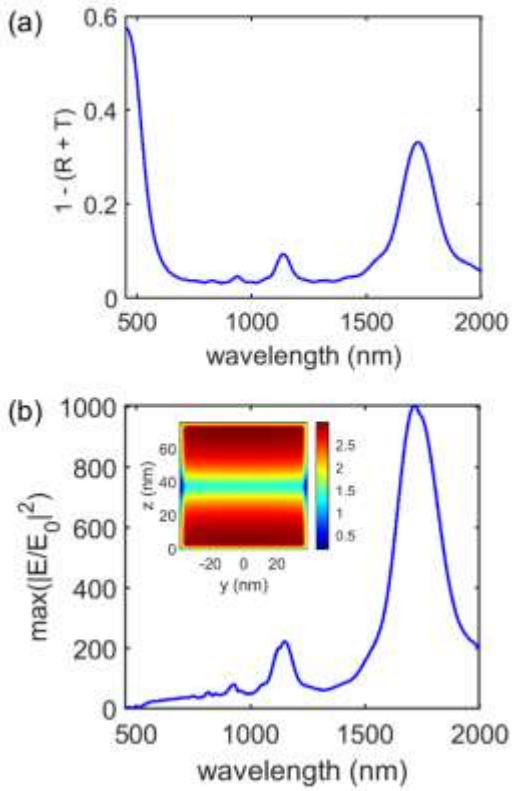

Fig. 8. Absorbance (a) and electric field intensity enhancement (b) of 75 nm gold nanoparticle array. The inset in (b) shows the intensity profile in log scale at the resonance wavelength of 1727 nm.

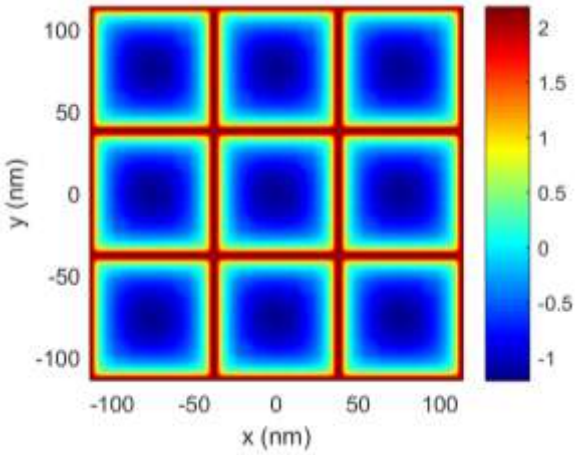

Fig. 9. Electric field intensity in log scale at λ = 1690 nm, 0.2 nm above the surface of the 75 nm nanocube array. The gap size is 1 nm and the incident light is unpolarized. The field profile forms a hot-grid.

IV. Conclusion

The MIM nanocube array presented in this work demonstrates a platform for achieving strong, localized electric field enhancement over large surface areas. By utilizing the interference of SPP mode in a Fabry-Pérot-like cavity, the structure enables intense, large area field enhancement without complex nanofabrication. This "hot-grid" design uniquely offers: (i) >1000-fold field enhancement over a large surface area, (ii) tunable optical response via nanoparticle size and material choice, (iii) extremely large wavevectors enabled by precisely controlled nanogaps, and (iv) suggests low-cost and scalable fabrication using bottom-up assembly methods. These findings establish practical design rules for next-generation SERS substrates, nonlinear optics, and other photonic applications requiring large-area, high-field enhancement.

References

[1] V. T. Tran, H.-Q. Nguyen, Y.-M. Kim, G. Ok, and J. Lee, "Photonic–Plasmonic Nanostructures for Solar Energy Utilization and Emerging Biosensors," *Nanomaterials*, vol. 10, no. 11, p. 2248, Nov. 2020, doi: 10.3390/nano10112248.

[2] L. Y. T. Nguyen, Y.-H. Lee, Y.-F. Chang, C.-C. Hsu, J.-Y. Lin, and H.-C. Kan, "Subwavelength-resolution imaging of surface plasmon polaritons with up-conversion fluorescence microscopy," *Opt. Express*, vol. 30, no. 2, pp. 3113–3124, Jan. 2022, doi: 10.1364/OE.449147.

[3] H. A. Atwater and A. Polman, "Plasmonics for improved photovoltaic devices," *Nat. Mater.*, vol. 9, no. 3, pp. 205–213, Mar. 2010, doi: 10.1038/nmat2629.

[4] H. Yu, Y. Peng, Y. Yang, and Z.-Y. Li, "Plasmon-enhanced light–matter interactions and applications," *Npj Comput. Mater.*, vol. 5, no. 1, pp. 1–14, Apr. 2019, doi: 10.1038/s41524-019-0184-1.

[5] R. H. Ritchie, "Surface plasmons in solids," *Surf. Sci.*, vol. 34, no. 1, pp. 1–19, Jan. 1973, doi: 10.1016/0039-6028(73)90183-0.

[6] Y. Fang and M. Sun, "Nanoplasmonic waveguides: towards applications in integrated nanophotonic circuits," *Light Sci. Appl.*, vol. 4, no. 6, pp. e294–e294, Jun. 2015, doi: 10.1038/lsa.2015.67.

[7] R. Zakaria, M. Mahbub, and C. S. Lim, "Studies of surface plasmon resonance effect on different metallic layers of silver (Ag) and copper (Cu) with molybdenum trioxide (MoO3) for formaldehyde sensor," *Results Opt.*, vol. 11, p. 100374, May 2023, doi: 10.1016/j.rio.2023.100374.

[8] K. A. Willets and R. P. V. Duyne, "Localized Surface Plasmon Resonance Spectroscopy and Sensing," *Annu. Rev. Phys. Chem.*, vol. 58, no. Volume 58, 2007, pp. 267–297, May 2007, doi: 10.1146/annurev.physchem.58.032806.104607.

[9] A. Lee *et al.*, "Probing Dynamic Generation of Hot-Spots in Self-Assembled Chains of Gold Nanorods by Surface-Enhanced Raman Scattering," *J. Am. Chem. Soc.*, vol. 133, no. 19, pp. 7563–7570, May 2011, doi: 10.1021/ja2015179.

[10] A. Ahmed and R. Gordon, "Single Molecule Directivity Enhanced Raman Scattering using Nanoantennas," *Nano Lett.*, vol. 12, no. 5, pp. 2625–2630, May 2012, doi: 10.1021/nl301029e.

[11] A. Ahmed and R. Gordon, "Directivity Enhanced Raman Spectroscopy Using Nanoantennas," *Nano Lett.*, vol. 11, no. 4, pp. 1800–1803, Apr. 2011, doi: 10.1021/nl200461w.

[12] A. Lee *et al.*, "Side-by-Side Assembly of Gold Nanorods Reduces Ensemble-Averaged SERS Intensity," *J. Phys. Chem. C*, vol. 116, no. 9, pp. 5538–5545, Mar. 2012, doi: 10.1021/jp3010597.

[13] J. Zhang, W. Zhao, P. Yu, G. Yang, and Z. Liu, "Second harmonic generation in 2D layered materials," *2D Mater.*, vol. 7, no. 4, p. 042002, Sep. 2020, doi: 10.1088/2053-1583/abaf68.

[14] G. Hajisalem, A. Ahmed, Y. Pang, and R. Gordon, "Plasmon hybridization for enhanced nonlinear optical response," *Opt. Express*, vol. 20, no. 28, pp. 29923–29930, Dec. 2012, doi: 10.1364/OE.20.029923.

[15] L. K. Sørensen *et al.*, "Nature of the Anomalous Size Dependence of Resonance Red Shifts in Ultrafine Plasmonic Nanoparticles," *J. Phys. Chem. C*, vol. 126, no. 39, pp. 16804–16814, Oct. 2022, doi: 10.1021/acs.jpcc.2c03738.

[16] R. Rastogi, E. A. Dogbe Foli, R. Vincent, P.-M. Adam, and S. Krishnamoorthy, "Engineering Electromagnetic Hot-Spots in Nanoparticle Cluster Arrays on Reflective Substrates for Highly Sensitive Detection of (Bio)molecular Analytes," *ACS Appl. Mater. Interfaces*, vol. 13, no. 28, pp. 32653–32661, Jul. 2021, doi: 10.1021/acsami.1c01953.

[17] P. Dey, V. Baumann, and J. Rodríguez-Fernández, "Gold Nanorod Assemblies: The Roles of Hot-Spot Positioning and Anisotropy in Plasmon Coupling and SERS," *Nanomaterials*, vol. 10, no. 5, Art. no. 5, May 2020, doi: 10.3390/nano10050942.

[18] F. Chen *et al.*, "Material influence on hot spot distribution in the nanoparticle heterodimer on film," *Phys. E Low-Dimens. Syst. Nanostructures*, vol. 98, pp. 1–5, Apr. 2018, doi: 10.1016/j.physe.2017.12.007.

[19] H. Wei *et al.*, "Plasmon Waveguiding in Nanowires," *Chem. Rev.*, vol. 118, no. 6, Art. no. 6, Mar. 2018, doi: 10.1021/acs.chemrev.7b00441.

[20] N. Yang, T.-T. You, Y.-K. Gao, C.-M. Zhang, and P.-G. Yin, "Fabrication of a Flexible Gold Nanorod Polymer Metafilm via a Phase Transfer Method as a SERS Substrate for Detecting Food Contaminants," *J. Agric. Food Chem.*, vol. 66, no. 26, pp. 6889–6896, Jul. 2018, doi: 10.1021/acs.jafc.8b01702.

[21] S. V. Sheen Mers, S. Umadevi, and V. Ganesh, "Controlled Growth of Gold Nanostars: Effect of Spike Length on SERS Signal Enhancement," *ChemPhysChem*, vol. 18, no. 10, pp. 1358–1369, 2017, doi: 10.1002/cphc.201601380.

[22] J. Doak, R. K. Gupta, K. Manivannan, K. Ghosh, and P. K. Kahol, "Effect of particle size distributions on absorbance spectra of gold nanoparticles," *Phys. E Low-Dimens. Syst. Nanostructures*, vol. 42, no. 5, pp. 1605–1609, Mar. 2010, doi: 10.1016/j.physe.2010.01.004.

[23] J. Liu *et al.*, "Recent Advances of Plasmonic Nanoparticles and their Applications," *Materials*, vol. 11, no. 10, p. 1833, Sep. 2018, doi: 10.3390/ma11101833.

[24] C. Zhu, X. Hu, and X. Wang, "Silver nanocubes/graphene oxide hybrid film on a hydrophobic surface for effective molecule concentration and sensitive SERS detection," *Appl. Surf. Sci.*, vol. 470, pp. 423–429, Mar. 2019, doi: 10.1016/j.apsusc.2018.11.169.

[25] J. Heintz, F. Legittimo, and S. Bidault, "Dimers of Plasmonic Nanocubes to Reach Single-Molecule Strong Coupling with High Emission Yields," *J. Phys. Chem. Lett.*, vol. 13, no. 51, pp. 11996–12003, Dec. 2022, doi: 10.1021/acs.jpclett.2c02872.

[26] H.-C. Hu, S.-H. Wu, L.-X. Jin, and J.-J. Sun, "Plasmonic Au nanocube enhanced SERS biosensor based on heated electrode and strand displacement amplification for highly sensitive detection of Dam methyltransferase activity," *Biosens. Bioelectron.*, vol. 210, p. 114283, Aug. 2022, doi: 10.1016/j.bios.2022.114283.

[27] L. Tian *et al.*, "Rational Approach to Plasmonic Dimers with Controlled Gap Distance, Symmetry, and Capability of Precisely Hosting Guest Molecules in Hotspot Regions," *J. Am. Chem. Soc.*, vol. 143, no. 23, pp. 8631–8638, Jun. 2021, doi: 10.1021/jacs.0c13377.

[28] W. Li, P. H. C. Camargo, X. Lu, and Y. Xia, "Dimers of Silver Nanospheres: Facile Synthesis and Their Use as Hot Spots for Surface-Enhanced Raman Scattering," *Nano Lett.*, vol. 9, no. 1, pp. 485–490, Jan. 2009, doi: 10.1021/nl803621x.

[29] A. Dhawan, S. J. Norton, M. D. Gerhold, and T. Vo-Dinh, "Comparison of FDTD numerical computations and analytical multipole expansion method for plasmonics-active nanosphere dimers," *Opt. Express*, vol. 17, no. 12, pp. 9688–9703, Jun. 2009, doi: 10.1364/OE.17.009688.

[30] R. Esteban *et al.*, "The Morphology of Narrow Gaps Modifies the Plasmonic Response," *ACS Photonics*, vol. 2, no. 2, pp. 295–305, Feb. 2015, doi: 10.1021/ph5004016.

[31] M. Kim, H. Kwon, S. Lee, and S. Yoon, "Effect of Nanogap Morphology on Plasmon Coupling," *ACS Nano*, vol. 13, no. 10, pp. 12100–12108, Oct. 2019, doi: 10.1021/acsnano.9b06492.

[32] R. Peng, T. Zhang, S. Yan, Y. Song, X. Liu, and J. Wang, "Recent Development and Applications of Stretchable SERS Substrates," *Nanomaterials*, vol. 13, no. 22, p. 2968, Nov. 2023, doi: 10.3390/nano13222968.

[33] P. Sultana, B. Qian, C. Son, S. Kim, G. Mensing, and P. Ferreira, "High-Volume Production of Repeatable High Enhancement SERS Substrates Using Solid-State Superionic Stamping," *J. Manuf. Sci. Eng.*, vol. 146, no. 110908, Sep. 2024, doi: 10.1115/1.4066398.

[34] P. Varasteanu *et al.*, "Close-packed small nanocubes assemblies as efficient SERS substrates," *J. Mol. Struct.*, vol. 1294, p. 136441, Dec. 2023, doi: 10.1016/j.molstruc.2023.136441.

[35] Z. Ye, C. Li, Q. Chen, Y. Xu, and S. E. J. Bell, "Self-assembly of colloidal nanoparticles into 2D arrays at water–oil interfaces: rational construction of stable SERS substrates with accessible enhancing surfaces and tailored plasmonic response," *Nanoscale*, vol. 13, no. 12, pp. 5937–5953, 2021, doi: 10.1039/D0NR08803J.

[36] J. Son, G.-H. Kim, Y. Lee, C. Lee, S. Cha, and J.-M. Nam, "Toward Quantitative Surface-Enhanced Raman Scattering with Plasmonic Nanoparticles: Multiscale View on Heterogeneities in Particle Morphology, Surface Modification, Interface, and Analytical Protocols," *J. Am. Chem. Soc.*, vol. 144, no. 49, pp. 22337–22351, Dec. 2022, doi: 10.1021/jacs.2c05950.

[37] M. E. Mann, P. Yadav, and S. Kim, "Colloidal Plasmonic Nanocubes as Capacitor Building Blocks for Multidimensional Optical Metamaterials: A Review," *ACS Appl. Nano Mater.*, vol. 4, no. 10, pp. 9976–9984, Oct. 2021, doi: 10.1021/acsanm.1c02211.

[38] J. T. Fourkas *et al.*, "Grand Challenges in Nanofabrication: There Remains Plenty of Room at the Bottom," *Front. Nanotechnol.*, vol. 3, no. 700849, 2021, doi: 10.3389/fnano.2021.700849.

[39] A. Klinkova *et al.*, "Structural and Optical Properties of Self-Assembled Chains of Plasmonic Nanocubes," *Nano Lett.*, vol. 14, no. 11, pp. 6314–6321, Nov. 2014, doi: 10.1021/nl502746h.

[40] X. Li *et al.*, "Printable assemblies of perovskite nanocubes on meter-scale panel," *Sci. Adv.*, vol. 8, no. 45, p. eadd1559, Nov. 2022, doi: 10.1126/sciadv.add1559.

[41] S. Gravelsins *et al.*, "Large emergent optoelectronic enhancement in molecularly cross-linked gold nanoparticle nanosheets," *Commun. Chem.*, vol. 5, no. 1, pp. 1–10, Aug. 2022, doi: 10.1038/s42004-022-00723-2.

[42] C. Moya, A. M. Abdelgawad, N. Nambiar, and S. A. Majetich, "Magnetic properties of cube-shaped Fe_3O_4 nanoparticles in dilute, 2D, and 3D assemblies," *J. Phys. Appl. Phys.*, vol. 50, no. 32, p. 325003, Aug. 2017, doi: 10.1088/1361-6463/aa7b11.

[43] B. Prade, J. Y. Vinet, and A. Mysyrowicz, "Guided optical waves in planar heterostructures with negative dielectric constant," *Phys. Rev. B*, vol. 44, no. 24, pp. 13556–13572, Dec. 1991, doi: 10.1103/PhysRevB.44.13556.

[44] S. A. Maier, *Plasmonics: Fundamentals and Applications*. Springer Science & Business Media, 2007.

[45] T. Wen and S. A. Majetich, "Ultra-Large-Area Self-Assembled Monolayers of Nanoparticles," *ACS Nano*, vol. 5, no. 11, pp. 8868–8876, Nov. 2011, doi: 10.1021/nn2037048.

[46] V. Santhanam, J. Liu, R. Agarwal, and R. P. Andres, "Self-Assembly of Uniform Monolayer Arrays of Nanoparticles," *Langmuir*, vol. 19, no. 19, pp. 7881–7887, Sep. 2003, doi: 10.1021/la0341761.

[47] T. W. Ebbesen, H. J. Lezec, H. F. Ghaemi, T. Thio, and P. A. Wolff, "Extraordinary optical transmission through sub-wavelength hole arrays," *Nature*, vol. 391, no. 6668, pp. 667–669, Feb. 1998, doi: 10.1038/35570.

[48] K. G. Lee and Q.-H. Park, "Coupling of Surface Plasmon Polaritons and Light in Metallic Nanoslits," *Phys. Rev. Lett.*, vol. 95, no. 10, p. 103902, Sep. 2005, doi: 10.1103/PhysRevLett.95.103902.

[49] I. R. Hooper and J. R. Sambles, "Dispersion of surface plasmon polaritons on short-pitch metal gratings," *Phys. Rev. B*, vol. 65, no. 16, p. 165432, Apr. 2002, doi: 10.1103/PhysRevB.65.165432.

[50] P. B. Johnson and R. W. Christy, "Optical Constants of the Noble Metals," *Phys. Rev. B*, vol. 6, no. 12, pp. 4370–4379, Dec. 1972, doi: 10.1103/PhysRevB.6.4370.

[51] G. Mie, "Beiträge zur Optik trüber Medien, speziell kolloidaler Metallösungen," *Ann. Phys.*, vol. 330, no. 3, pp. 377–445, 1908, doi: 10.1002/andp.19083300302.

[52] S. Zhang, K. Bao, N. J. Halas, H. Xu, and P. Nordlander, "Substrate-Induced Fano Resonances of a Plasmonic Nanocube: A Route to Increased-Sensitivity Localized Surface Plasmon Resonance Sensors Revealed," *Nano Lett.*, vol. 11, no. 4, pp. 1657–1663, Apr. 2011, doi: 10.1021/nl200135r.